Supplementary Information

Exploiting Conjugated Polyelectrolyte Photophysics towards Monitoring Real-Time Lipid Membrane-Surface Interaction Dynamics at the Single Particle Level

*Christina F. Calver, Hsiao-Wei Liu, and Gonzalo Cosa**

Department of Chemistry and Centre for Self Assembled Chemical Structures (CSACS/CRMAA), McGill University, 801 Sherbrooke Street West, Montreal, QC, H3A 0B8, Canada

***To whom correspondence should be addressed**

E-mail: gonzalo.cosa@mcgill.ca

This Supplementary information section includes:

1. Characterization of SiO_2 nanoparticle size after functionalization with (3-aminopropyl)trimethoxysilane and adsorption of MPS-PPV
2. Characterization of MPS-PPV coated NPs by UV-vis and fluorescence spectroscopy
3. Normalized emission spectra of MPS-PPV coated NPs before and after addition to DOTAP liposomes
4. Non-specific adsorption of DOTAP liposomes on aminosilanized glass coverslips in the context of TIRFM studies
5. Histogram of MPS-PPV coated NP enhancements obtained from TIRFM studies where DOTAP liposomes were flowed at high concentration
6. Comparison of the MPS-PPV coated NP size distribution and the fluorescence intensity distribution of individual NPs
7. Dye leakage experiments of Cy5 fluorophores encapsulated inside DOTAP liposomes to determine extent of liposome rupture

Characterization of nanoparticles by transmission electron microscopy and dynamic light scattering

Particle size was determined after each modification step by transmission electron microscopy (TEM) and dynamic light scattering (DLS). The TEM images did not show an appreciable change in the particle core size or appearance after either the aminosilanization or the MPS-PPV adsorption steps (Figure S1). DLS measurements showed no change after aminosilanization of the SiO_2 NPs. Upon adsorption of MPS-PPV on SiO_2NH_3+ the size distribution broadened and shifted toward larger sizes. (Figure S2). Although MPS-PPV is a water-soluble polymer, it has a tendency to adopt a self-aggregated conformation in water, likely due to considerable contributions from its hydrophobic backbone. This aggregation, or possibly polymer bridging between several MPS-PPV coated nanoparticles could explain the increased size.

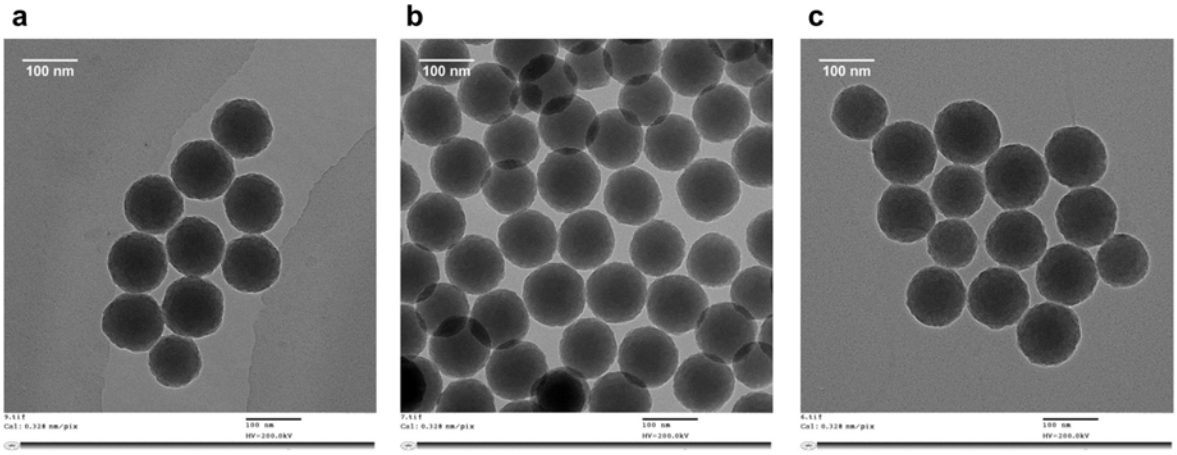

Figure S1. Transmission electron micrographs of a) SiO_2 NPs, b) $SiO_2NH_3^+$ NPs, and c) MPS-PPV coated $SiO_2NH_3^+$ NPs. The mean core sizes were 111 (±8) nm, 104 (±12) nm, and 108 (±10) nm, respectively. Scale bar = 100 nm.

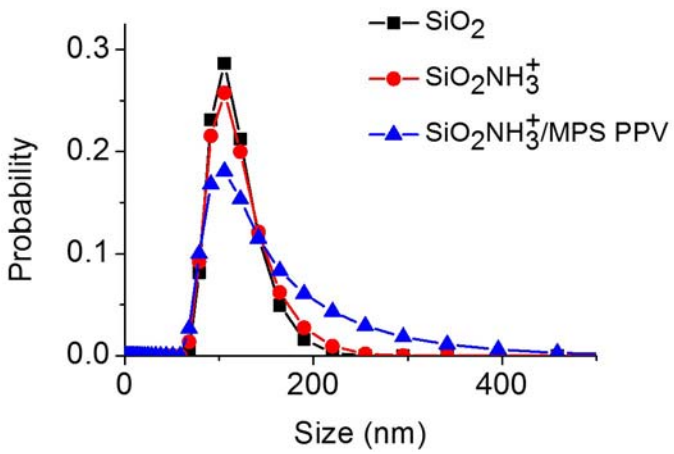

Figure S2. Size distributions of SiO_2 NPs, $SiO_2NH_3^+$ NPs, and MPS-PPV coated $SiO_2NH_3^+$ NPs as determined by dynamic light scattering measurements.

Characterization of MPS-PPV coated SiO_2 NPs by UV-vis absorption spectroscopy

In order to determine the amount of MPS-PPV adsorbed on the NPs, the UV-vis absorbance spectra of $SiO_2NH_3^+$ NPs and MPS-PPV coated $SiO_2NH_3^+$ NPs at equal concentrations were acquired (Figure S3). The absorbance spectrum of the MPS-PPV coated NPs contained contributions from both the scattering of the SiO_2 NPs and the absorbance of MPS-PPV. In order to deconvolute the spectrum into these two components, the absorbance spectrum of the $SiO_2NH_3^+$ NPs was subtracted from the spectrum of the MPS-PPV coated NPs to remove the contribution due to scattering. The spectrum remaining after subtraction resembled the spectrum of unadsorbed (free) MPS-PPV. Using Beer's Law and an extinction coefficient of 3460 $M^{-1}cm^{-1}$ per polymer repeat unit, the concentration of MPS-PPV was calculated to be 13 μM. Considering that the NP concentration in the sample was 13 nM, the number of polymer repeat units per NP was determined to be approximately 100,000. The surface area of one MPS-PPV monomer unit was estimated to be 0.36 nm^2 and the total polymer surface area per particle

is then 36,000 nm^2. Given that the surface area of a sphere with r = 50 nm is 31,000 nm^2, there is enough MPS-PPV adsorbed onto the particles to cover the surface approximately 1.2 times.

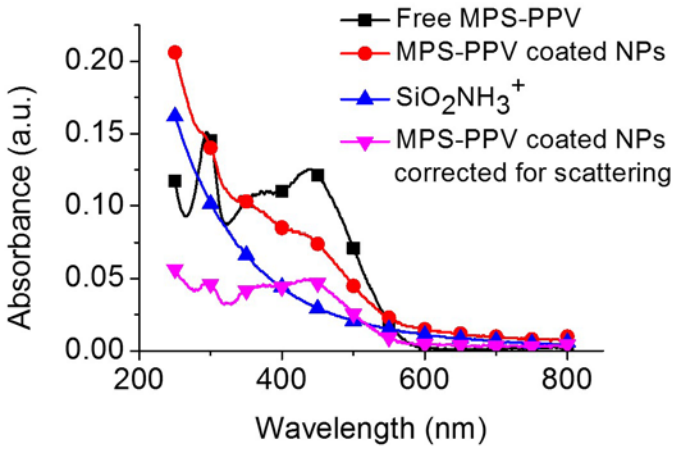

Figure S3. Absorbance spectra of 0.13 nM $SiO_2NH_3^+$ NPs and 0.13 nM MPS-PPV coated NPs in water (blue triangles and red circles, respectively). The spectrum of the $SiO_2NH_3^+$ NPs was subtracted from the spectrum of the MPS-PPV coated NPs to correct for the contribution of scattering to the spectrum (inverted purple triangles). The subtracted spectrum is qualitatively similar to the spectrum of free MPS-PPV, as expected (black squares).

Characterization of MPS-PPV coated SiO_2 NPs by ensemble fluorescence spectroscopy

The emission spectrum of the MPS-PPV coated SiO_2 NPs and the emission spectrum of free MPS-PPV were acquired and then compared. There were no spectral differences between the emission spectrum of adsorbed and non-adsorbed MPS-PPV but the emission intensity is quenched 66% upon adsorption onto the nanoparticle (Figure S4). The promotion of increased interchain contacts by the NP scaffolding likely increases the amount of polymer self-quenching by increasing the efficiency of exciton hopping to non-emissive trap sites.

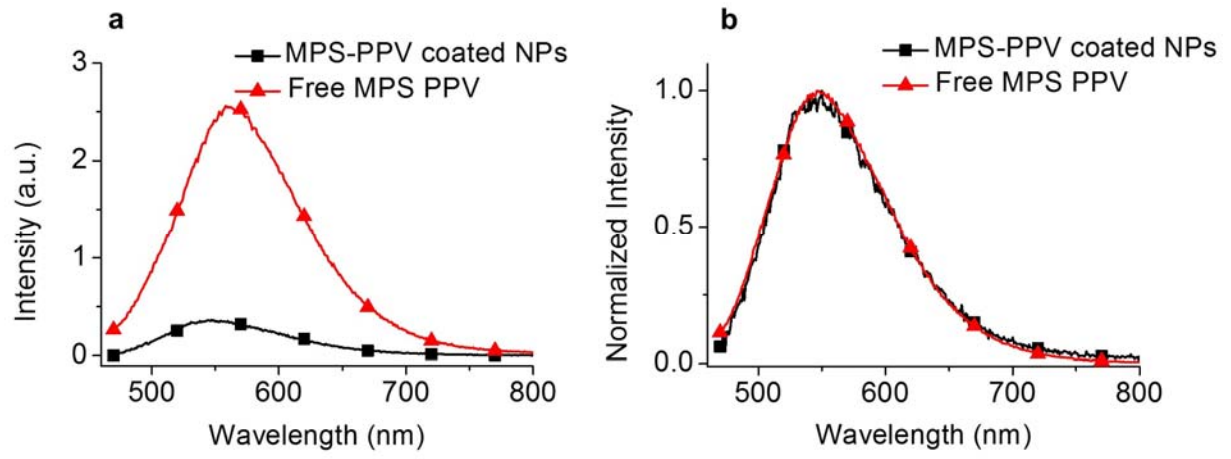

Figure S4. a) Emission spectrum of MPS-PPV coated NPs (black squares) and free MPS-PPV (red triangles) in 3 mM NaCl. b) Normalized emission spectra of MPS-PPV coated NPs (black squares) and free MPS-PPV (red triangles) emphasize that the emission profile of MPS-PPV is unchanged upon adsorption on the NP support. The excitation wavelength was 450 nm for all samples.

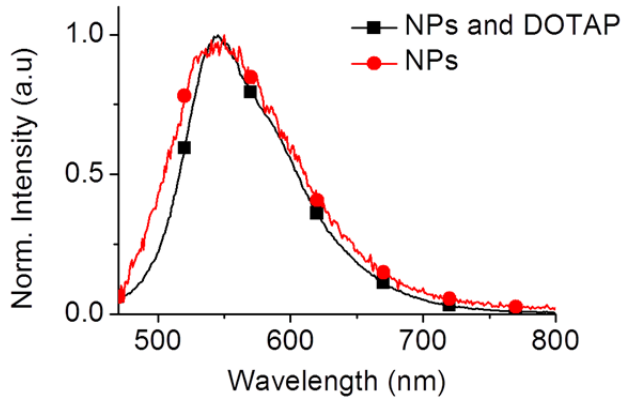

Figure S5. Normalized emission spectra of 0.1 nM MPS-PPV coated NPs before (red circles) and after (black squares) addition to 13 nM 100 nm DOTAP liposomes in 3 mM NaCl. Spectra are the same as those shown in Figure 1A. The excitation wavelength was 450 nm.

Determining the correct solution ionic strength to prevent non-specific adsorption of DOTAP liposomes on aminosilanized glass coverslips for TIRFM studies

In order to ensure that the interaction between the NPs and the liposomes observed during TIRFM experiments was specific, control experiments with dye-labelled liposomes were performed to assess the extent of non-specific liposome adsorption on the surface. A total of 20 µL of 100 µM DOTAP (400 nm liposomes) containing the red emitting, lipophilic dye DiD in a lipid to dye ratio of 256:1 were injected into the imaging chamber. The liposomes were incubated for five minutes and then the chamber was rinsed with a solution having the same NaCl concentration. The surface was then imaged to determine the extent of non-specific liposome adsorption (Figure S5). The adsorption of liposomes on the surface was first observed at a NaCl concentration of 4 mM (B), with the number of adsorbed liposomes greatly increasing as the NaCl concentration was increased to 50 mM (C). For this reason, experiments were conducted at 3 mM NaCl (A) to minimize the non-specific adsorption of liposomes on the surface.

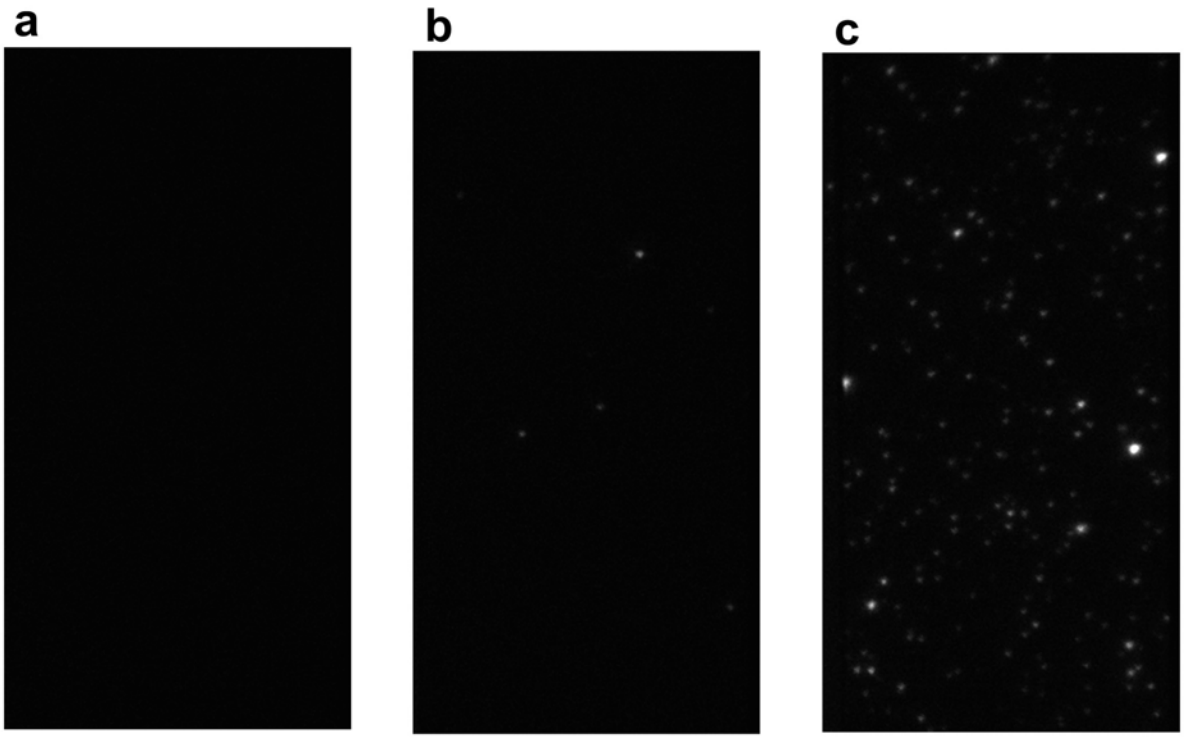

Figure S6. Non-specific adsorption of DOTAP liposomes after five minutes of incubation on a aminosilanized glass coverslips in solution conditions of a) 3 mM NaCl, b) 4 mM NaCl, and c) 50 mM NaCl.

Enhancement of MPS-PPV adsorbed on SiO_2 NPs when DOTAP liposomes are flowed at a high concentration

DOTAP liposomes 100 nm and 400 nm in diameter were flowed over surface-immobilized MPS-PPV coated NPs at high liposome concentrations of 13 and 8 nM, respectively. Both the mean enhancement (23-fold and 22-fold, respectively) and the distribution of enhancements (Figure S7) were indistinguishable between the two liposome samples. According to our model, liposomes adsorb on the surface of the MPS-PPV coated NPs causing the deaggregation of MPS-PPV and its concomitant fluorescence enhancement. Under these conditions, liposomes were present in excess such that the surface of the NPs was

passivated with adsorbed liposomes and the enhancements observed were maximal. The fact that the 100 nm and 400 nm populations are indistinguishable is consistent with this model in that the size of the liposome does not dictate the extent of the NP emission enhancement so long as MPS-PPV has access to an excess of lipids. The small percentage of outliers (<5%) lying at enhancement values > 50 can be explained by considering that the calculation of the enhancement is particularly sensitive to errors in the determination of the initial intensity. Given the limited dynamic range of the CCD camera, it was necessary to start with a low initial intensity in order to capture the large emission enhancements. An underestimation of the initial intensity could lead to artificially high enhancements as these values were close to the background intensity level. Indeed, the top 5% of enhancements were found to have an average initial intensity of 44±16 which was significantly lower than the average initial intensity of all particles at 81±43. Despite the existence of several outliers, the mean enhancement for both samples agreed well with the enhancement determined in ensemble fluorescence studies.

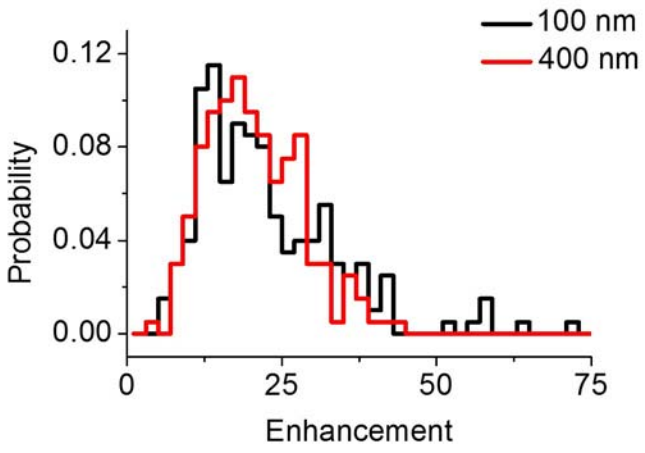

Figure S7. Histogram of enhancement values recorded for MPS-PPV coated NPs observed while flowing 100 nm and 400 nm DOTAP liposomes at a high liposome concentration of 13

and 8 nM, respectively. Enhancement values shown in the histogram were determined from the fluorescence intensity versus time trajectories of 200 MPS-PPV coated NPs for both conditions.

Distribution of single MPS-PPV coated NP intensities

The amount of MPS-PPV adsorbed onto the SiO_2 NPs was expected to depend on the surface area of the underlying SiO_2 support. The distribution of MPS-PPV coated NP fluorescence intensities observed during TIRFM experiments was related to the distribution of MPS-PPV coated NP sizes obtained by dynamic light scattering measurements (Figure S8).

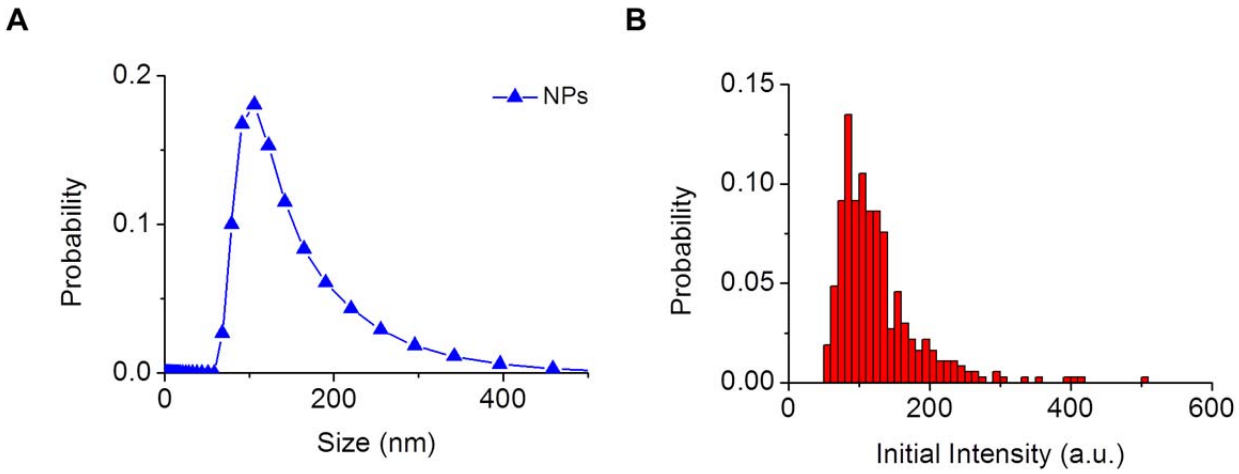

Figure S8. A) Size distribution of MPS-PPV coated $SiO_2NH_3^+$ NPs determined by dynamic light scattering. B) Histogram of the initial fluorescence intensity values recorded for 371 individual MPS-PPV coated NPs during TIRFM experiments.

Monitoring the rupture of DOTAP liposomes in contact with MPS-PPV coated NPs

A dye leakage experiment with the red-emitting fluorophore sulfo-Cy5 carboxylic acid was performed to provide additional evidence that the majority of DOTAP liposomes do not rupture upon adsorption onto the MPS-PPV coated NPs over the timescale observed during the

TIRFM experiments. Cy5 was encapsulated within DOTAP liposomes suspended in a solution of the quencher $FeCl_3$. Positively charged Fe^{3+} ions cannot cross the DOTAP membrane but are present in sufficient amount to efficiently quench the emission of the encapsulated fluorophores if the membrane ruptures and releases them into solution. MPS-PPV coated NPs were added to a $FeCl_3$ solution containing DOTAP liposomes with encapsulated Cy5 molecules. The emission spectrum of Cy5 was measured immediately and ten minutes after mixing (Figure S9). Only a slight quenching of the Cy5 emission was observed, which was consistent with relatively slow liposome rupture kinetics under these conditions. In order to prove that the assay was capable of detecting liposome rupture, the liposomes were exposed to conditions that mechanically disrupted the membrane. The mixture of DOTAP, NPs, and $FeCl_3$ was frozen on dry ice (5 min) and then thawed in a water bath (5 min). After this cycle the fluorescence intensity was nearly completely quenched, consistent with liposome rupture rendering the contents vulnerable to quenching by $FeCl_3$

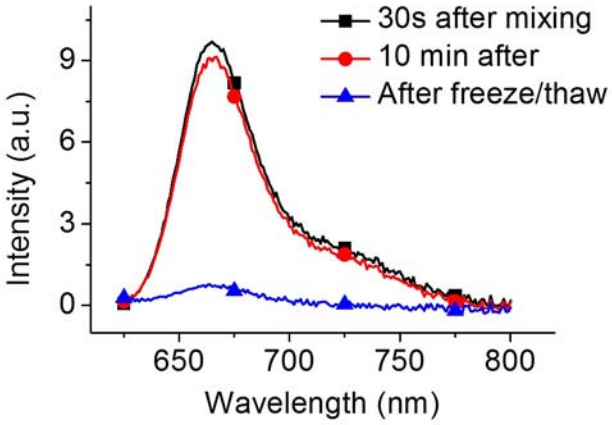

Figure S9. Emission intensity of the fluorophore sulfo-Cy5 carboxylic acid initially encapsulated inside of 100 nm DOTAP liposomes at a density of 100 Cy5 per liposome. A 1.1 nM liposome solution in 300 µM $FeCl_3$ was mixed with 0.11 nM MPS-PPV coated NPs. The

Cy5 emission spectrum was recorded 30 s (black squares) and 10 min (red circles) after mixing. Also shown is the spectrum of an identical solution that was frozen on dry ice to mechanically disrupt the membrane upon thawing to room temperature (blue triangles). The excitation wavelength was 600 nm for all samples.